Plasma Sources
Science and
Technology

PAPER • **OPEN ACCESS**

Anisotropic quasi-atomic layer etching of $InGaZnO_4$ using unbiased CH_4 and continuous/pulsed biased O_2 plasmas

To cite this article: Jie Li *et al* 2026 *Plasma Sources Sci. Technol.* **35** 025033

Plasma Sources Science and Technology

PAPER

OPEN ACCESS

RECEIVED
23 October 2025

REVISED
26 January 2026

ACCEPTED FOR PUBLICATION
18 February 2026

PUBLISHED
27 February 2026

Anisotropic quasi-atomic layer etching of $InGaZnO_4$ using unbiased CH_4 and continuous/pulsed biased O_2 plasmas

Jie Li*, Shreya Kundu, Laurent Souriau, Hendrik F W Dekkers, Yiqun Wan, Thierry Conard, Attilio Belmonte and Katia Devriendt

Interuniversity Microelectronics Centre (IMEC), Heverlee 3001, Belgium
* Author to whom any correspondence should be addressed.

E-mail: li17@imec.be

Keywords: IGZO, ALE, CH_4 plasma, O_2 plasma, cation composition, ALE process window, ALE synergy

Abstract

In this study, an anisotropic quasi-atomic layer etching (qALE) process for $InGaZnO_4$ (IGZO) removal was developed and systematically investigated, consisting of alternating unbiased CH_4 plasma adsorption and biased (continuous or pulsed) O_2 plasma desorption steps. The etching behavior was examined by independently varying the CH_4 plasma time, O_2 plasma time, surface temperature, bias voltage, and pulse duty cycle. The total cyclic etch rate was analyzed in terms of its physical and chemical components, with the two etching contributions examined separately. The physical cyclic etch rate increased linearly with O_2 plasma processing time, bias voltage, and pulse duty cycle, while the chemical cyclic etch rate exhibited a self-limiting behavior with increasing CH_4 and O_2 plasma processing times. The chemical cyclic etch rate rose from 0.07 nm/cycle at 0% duty cycle in pulsed biased O_2 plasma to 0.13 nm/cycle at 10%, remained constant between 10% and 70%, and further increased to 0.20 nm/cycle at 100%. This defined a qALE process window between 10% and 70% duty cycle at 60 V bias voltage, likely due to the complete removal of the saturated hydrocarbonated IGZO layer under moderate ion bombardment. ALE synergy decreased with increasing O_2 plasma time, higher bias voltage, and higher duty cycle, reflecting the enhanced physical etching contribution. The cation composition of the IGZO film surface was analyzed using x-ray photoelectron spectroscopy after the qALE process. The Ga fraction in amorphous IGZO increased following qALE, due to the stronger Ga–O bond relative to In–O and Zn–O, resulting in a lower Ga etch rate. However, under higher bias voltage in the O_2 plasma step, the Ga enrichment was less pronounced, suggesting the formation and desorption of Ga-containing etch by-products at elevated ion bombardment. This developed anisotropic qALE process was effectively applied to top-gate trench patterning for IGZO channel transistor fabrication, enabling precise control of channel thickness and yielding an excellent etch profile with high ALE synergy.

1. Introduction

$InGaZnO_4$ (IGZO) has emerged as a promising candidate for next-generation semiconductor channel materials, offering higher carrier mobility, greater current density, and a wider bandgap compared to conventional amorphous silicon. IGZO-based transistors demonstrate extremely low off-currents and are compatible with large-area fabrication at low processing temperatures. Owing to these properties, IGZO is particularly well suited for applications in DRAM, compute-in-memory architectures, and BEOL integration in advanced semiconductor fabrication [1–5]. As IGZO devices continue to scale down, precise control over IGZO patterning during the device fabrication becomes increasingly critical. In particular, accurate regulation of the IGZO channel recess depth during etching is essential for ensuring reliable device performance.

Several studies have examined the plasma etching of IGZO thin films using different plasma chemistries. Halogen-containing plasmas such as CF_4, SF_6, and BCl_3 have been commonly employed, with etch behavior strongly influenced by process parameters including plasma power, bias power, and chamber pressure [6–12]. More recently, hydrocarbon-based plasmas have been investigated for IGZO patterning, as they provide higher etching selectivity over silicon and other contact materials, offering significant advantages for integration processes [13–15]. While reactive ion etching of IGZO has been widely reported, studies on atomic layer etching (ALE) remain limited. ALE is considered a more suitable technique for nanoscale IGZO patterning because it enables atomic-level precision, improved surface uniformity, reduced etch depth variation, and minimized plasma-induced damage. In our previous work, an isotropic ALE approach was proposed, involving alternating hydrocarbon plasma exposure and O radical treatment, where layer-by-layer IGZO removal was achieved through self-limiting surface hydrocarbonation followed by O radical mediated etching [16]. However, the anisotropic characteristics of this ALE process have not yet been explored, despite their critical importance for IGZO-based device fabrication.

In this work, the anisotropic etching characteristics of an ALE process combining cyclic unbiased CH_4 plasma and biased (both continuous and pulsed) O_2 plasma were investigated. The total etch rate was analyzed in terms of its physical and chemical components, and a self-limiting cyclic chemical etch rate was observed with increasing CH_4 plasma and O_2 plasma processing times. The effects of surface temperature, bias voltage, and pulse duty cycle on the physical and chemical etch characteristics, as well as the IGZO cation composition, were also examined. ALE synergy was evaluated under various process conditions, and the ALE process window was defined at specific bias conditions. Furthermore, this anisotropic ALE process was applied to the top gate trench patterning for IGZO channel transistor fabrication, achieving an excellent etch profile and precise control of the IGZO channel thickness with high ALE synergy.

2. Experimental section

Amorphous IGZO thin films, 50 nm thick, were deposited on 300 mm Si wafers via a physical vapor deposition (PVD) process. Prior to deposition, the substrates were degassed at 350 °C in an Ar atmosphere to remove residual moisture. Deposition was performed using an Ar/O_2 mixture plasma and a polycrystalline IGZO target (In:Ga:Zn = 1:1:1) in a PVD chamber (Applied Materials, Clover). The films were subsequently annealed at 350 °C in an O_2/N_2 atmosphere for 1 h to enhance film density. The cation composition of In:Ga:Zn in the films, determined by x-ray photoelectron spectroscopy (XPS), was 46%:30%:24%. The IGZO/Si bilayers were diced into 20 × 20 mm^2 samples, mounted at the center of 300 mm Si carrier wafers, and introduced into an inductively coupled plasma reactor (Lam Research, 2300 Kiyo GX) for the anisotropic quasi-ALE (qALE) process. This process consists of alternating CH_4 plasma adsorption and O_2 plasma desorption steps, as summarized in figure 1. During the adsorption step, CH_4 plasmas were generated with a source power of 800 W, bias power of 0 W, total flow rate of 100 sccm, and process pressure of 20 mTorr, with processing times ranging from 5 to 120 s. In the desorption step, O_2 plasmas were generated with a source power of 800 W, total flow rate of 200 sccm, and process pressure of 10 mTorr, with processing times between 10 and 300 s. Both continuous (0–150 V) and pulsed bias power (60 V, 1 kHz, duty cycle 0%–100%) were applied during desorption. The substrate surface temperature was varied from 20 °C to 140 °C. These steps were repeated for up to 50 cycles to etch the IGZO thin films.

The thickness of the IGZO films was measured using an ellipsometer (KLA Tencor, SpectraCD) before and after the qALE processes to determine the cyclic etch rate. The film surface was characterized by XPS following qALE processes. XPS measurements were performed using a spectrometer (Physical Electronics, Quantes) with a monochromatic Al-Kα (1486.6 eV) x-ray source, and binding energies were calibrated using the C 1s peak at 284.8 eV. The qALE process was further applied to pattern trenches for top-gate formation in IGZO-based DRAM device fabrication, and the resulting etch profile was characterized by transmission electron microscopy (TEM).

3. Results and discussion

The cyclic etch rate of IGZO thin films was evaluated as functions of CH_4 plasma processing time in the adsorption step and O_2 plasma processing time in the desorption step, as shown in figure 2. The physical etch rate was determined from O_2 plasma etching without CH_4 plasma modification, and the chemical contribution was obtained by subtracting the physical etch rate from the total etch rate. The physical, chemical, and total cyclic etch rates are presented in figure 1. As shown in figure 2(a), with

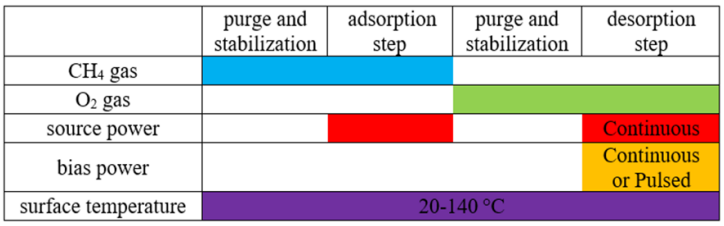

Figure 1. Sequence of one anisotropic quasi-ALE cycle for IGZO etching.

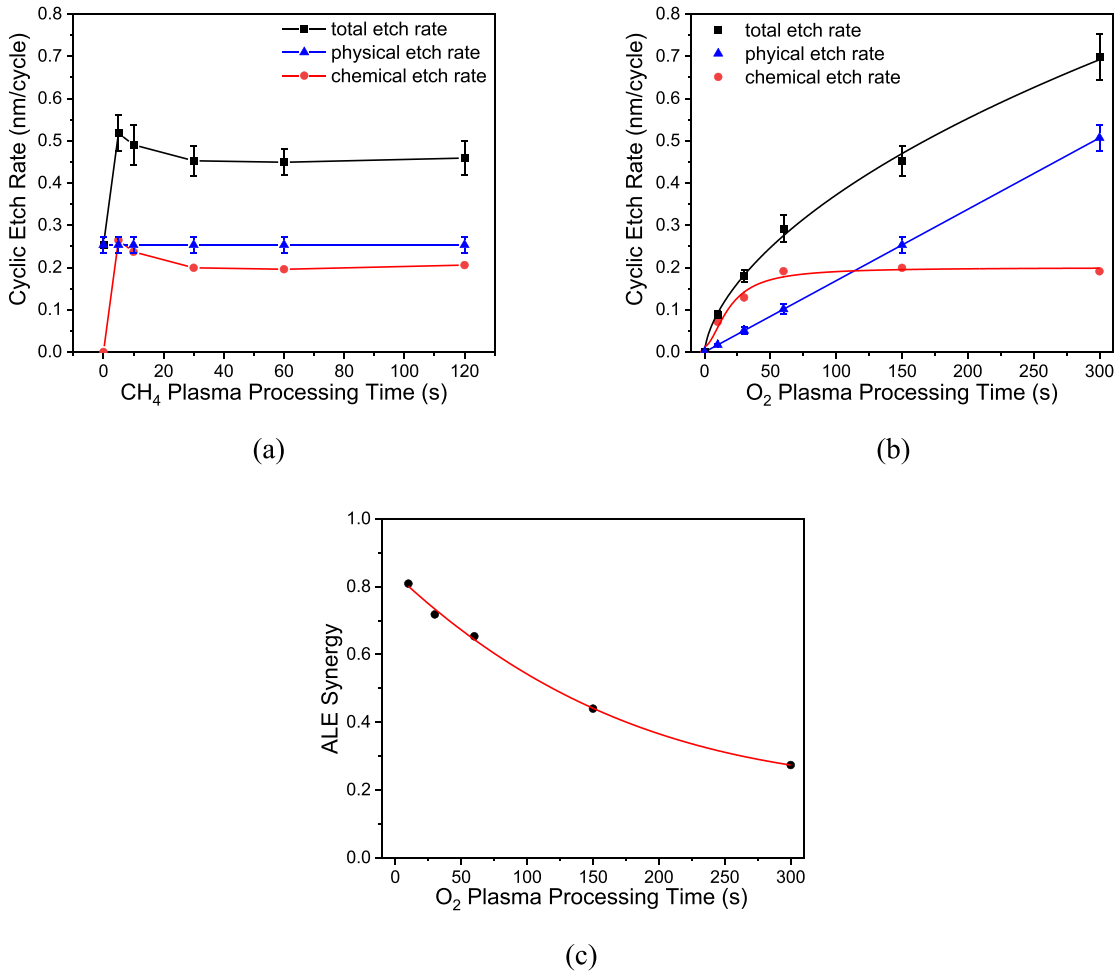

Figure 2. (a) IGZO cyclic etch rates (total, physical, and chemical) as a function of CH_4 plasma processing time, with continuous O_2 plasma step fixed at a 60 V bias voltage and a 150 s processing time. (b) IGZO cyclic etch rates (total, physical, and chemical) as a function of continuous O_2 plasma processing time at a 60 V bias voltage, with the CH_4 plasma step fixed at 30 s. (c) ALE synergy as a function of O_2 plasma processing time. The surface temperature was maintained at 140 °C in (a)–(c).

increasing CH_4 plasma time from 5 to 120 s, the total etch rate remained nearly constant at about 0.45 nm/cycle, which can be attributed to the self-limiting thickness of the hydrocarbonated IGZO layer, as demonstrated in our previous study [16]. During the CH_4 plasma step, hydrocarbon and hydrogen radicals penetrate the IGZO film and modify the pristine IGZO surface. The penetration depth increases with plasma exposure time but eventually saturates. In the subsequent O_2 plasma step, O radicals selectively remove only the modified IGZO layer, which leads to a self-limiting chemical cyclic etch rate. The slightly higher etch rates observed at CH_4 plasma processing times of 5 and 10 s are likely due to reduced hydrocarbon deposition on the IGZO surface, as excessive hydrocarbon deposition suppresses etching [15]. The physical and chemical cyclic etch rates were 0.25 nm/cycle and 0.20 nm/cycle, respectively, under continuous O_2 plasma with a 60 V bias voltage and a 150 s processing time in desorption step. The cyclic etch rate was investigated as a function of continuous O_2 plasma processing time, as shown in figure 2(b). The physical cyclic etch rate increased linearly with O_2 plasma time, while the

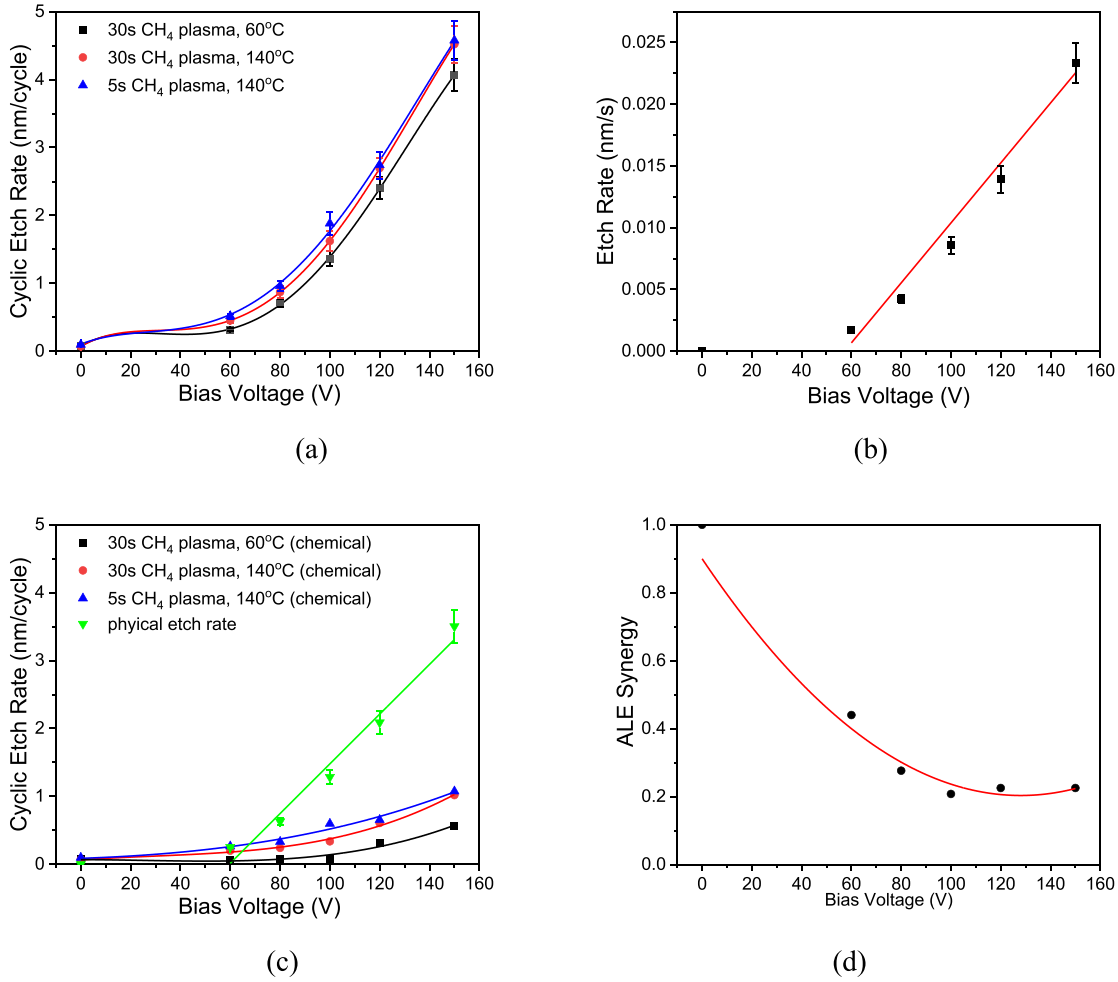

Figure 3. (a) IGZO total cyclic etch rate as a function of bias voltage in the continuous O_2 plasma step with a 150 s processing time. The substrate temperature and CH_4 plasma step processing time were varied. (b) IGZO etch rate in continuous O_2 plasma without the CH_4 plasma step. The surface temperature was maintained at 140 °C. (c) IGZO cyclic etch rates (physical and chemical) as a function of bias voltage in the O_2 plasma step with a 150 s processing time. (d) ALE synergy as a function of bias voltage in the O_2 plasma step. CH_4 plasma time was 30 s, O_2 plasma time was 150 s, and the surface temperature was maintained at 140 °C.

chemical cyclic etch rate rose to 0.19 nm/cycle at 60 s before saturating with further O_2 plasma exposure. This self-limiting behavior of the chemical cyclic etch rate is likely due to the complete removal of the hydrocarbonated IGZO layer. To evaluate the fraction of self-limiting etching in the total etching process, the ALE synergy was introduced and defined as follows [17]:

$$S = \frac{\mathrm{EPC} - (\alpha + \beta)}{\mathrm{EPC}} \tag{1}$$

where EPC represents the total etch rate per cycle, α denotes the amount of unintended etching during the adsorption step, β corresponds to the sputtering of unmodified material during the desorption step. In this study, α was set to 0 because the unbiased CH_4 plasma induced hydrocarbon deposition on the IGZO surface instead of material removal, and β was taken as the physical etch rate; thus, the ALE synergy (S) represents the ratio of the chemical etch rate to the total etch rate. The ALE synergies under different O_2 plasma processing times are shown in figure 2(c). ALE synergy decreased from 0.81 at 10 s to 0.27 at 300 s, due to the continued physical etching of unmodified IGZO after the hydrocarbonated IGZO layer had been chemically removed as metal-, carbon-, hydrogen-, and oxygen-containing by-products in O_2 plasmas [16].

The dependence of IGZO cyclic etch rate on bias voltage in continuous O_2 plasmas (desorption step) was investigated, as shown in figure 3. Under CH_4 plasma processing for 30 s and a substrate temperature of 140 °C, the total cyclic etch rate increased from 0.07 nm/cycle at a bias voltage of 0 V in O_2 plasma to 0.45 nm/cycle at 60 V, and further to 4.5 nm/cycle at 150 V, as shown in figure 3(a). The qALE process window for IGZO thin films, where the cyclic etch rate remains constant and independent

of bias voltage, is expected to lie between ion energies of 0 V and 60 V in O_2 plasmas. The slightly higher etch rate observed with a CH_4 processing time of 5 s is attributed to reduced hydrocarbon deposition, whereas the slightly lower etch rate at a substrate temperature of 60 °C is likely due to decreased surface reactivity and less efficient desorption of volatile etch by-products. IGZO physical etch rates in O_2 plasmas without CH_4 plasma pretreatment are shown in figure 3(b), and the physical and chemical cyclic etch rates are presented in figure 3(c). The physical cyclic etch rate was linearly proportional to bias voltage, consistent with previous studies [18], while the chemical cyclic etch rate increased with bias voltage, potentially due to enhanced formation and desorption of chemical etch by-products at higher ion energy. The ALE synergy decreased from 1.0 at 0 V to 0.21 at 100 V and remained nearly unchanged over the range from 100 V to 150 V, as shown in figure 3(d).

IGZO thin films were characterized by XPS measurements both prior to and after the qALE process, as summarized in figure 4(a). Core-level signals corresponding to O 1s (530.8 eV), In $3d_{5/2}$ (445.2 eV), Zn $2p_{3/2}$ (1022.0 eV), and Ga $2p_{3/2}$ (1118.0 eV) were detected [19, 20], and their corresponding high-resolution spectra are shown in figures 4(b)–(e). The O 1s spectrum (figure 4(b)) shows three distinct features: a low-binding-energy peak at 530.3 eV (O_L), an intermediate component at 531.2 eV (O_M), and a high-binding-energy feature at 532.4 eV (O_H). The O_L peak is commonly attributed to O^{2-} ions in a fully coordinated metal–oxygen network, whereas the O_M component is associated with O^{2-} ions in oxygen-deficient environments [21–31]. The O_H contribution is generally linked to surface hydroxyl species [21–25, 32]. However, some studies have reported that the O_M component can also originate from hydroxyl groups, carbonates, and adsorbed water [33–36]. In this manuscript, the O 1s peak shift is therefore treated only as a qualitative indicator of changes in oxygen-related defect states, rather than a quantitative measure of oxygen vacancy concentration. After the qALE treatment, the O 1s spectrum shifts from the O_L component toward higher binding energies, indicating an increase in oxygen-deficient sites within the IGZO film. This behavior is likely caused by interactions between lattice oxygen and hydrocarbon species during the CH_4 plasma adsorption step. As the O_2 plasma bias voltage increases during the desorption step, the extent of this shift is reduced, suggesting partial replenishment of oxygen vacancies through bombardment by energetic O_2^- ions. In addition, the shift toward O_H region implies the formation of hydroxyl-related bonds on the IGZO surface during the qALE process.

Shifts of the metal peaks toward higher binding energies after the qALE process were observed in the In $3d_{5/2}$, Zn $2p_{3/2}$, and Ga $2p_{3/2}$ spectra, as shown in figures 4(c)–(e). These shifts suggest possible structural changes of the metal–oxygen network induced by the etch process. After etching with higher O_2 bias voltages (100 V and 150 V), the metal peaks appear closer to those of the as-deposited IGZO thin films than after etching at lower O_2 bias voltages (0 V and 60 V). This reduced impact on the metal network at higher O_2 bias voltages is likely due to energetic O_2^+ ions partially replenishing oxygen vacancies, consistent with the changes observed in the O 1s spectrum.

The cation compositions of In, Ga, and Zn were quantified from peak areas and elemental sensitivity factors, as shown in figure 4(f). After the qALE process without bias voltage, the Ga fraction increased markedly from 29.8% to 62.3%, likely due to the higher Ga–O bond energy (2.0 eV) and its correspondingly lower etch rate compared with In–O (1.7 eV) and Zn–O (1.5 eV) in amorphous IGZO [37]. However, at higher O_2 bias voltages the Ga enrichment was less pronounced, suggesting that ion bombardment enhances the formation and desorption of Ga-containing etch by-products, likely volatile organometallic compounds such as $Ga(CH_3)_2$, as reported in the literature [38]. The In fraction decreased from 45.7% to 23.9% after the qALE process without bias voltage but rose to 53.8% at 150 V. The slower In etching at higher bias voltages indicates that its removal is primarily driven by radical reactions and less influenced by ion bombardment. The Zn fraction decreased steadily from 24.5% to 13.8% after qALE without bias voltage and further to 7.8% at 150 V, indicating an accelerated Zn etch rate with increasing ion bombardment.

The IGZO cyclic etch rate was also examined as a function of surface temperature, as shown in figure 5(a). With a 60 V bias voltage applied during the O_2 plasma desorption step, the total etch rate remained nearly constant at 0.32 nm/cycle from 20 °C to 60 °C, but increased to 0.41 nm/cycle at 80 °C. This increase at 80 °C is likely associated with the formation and desorption of additional volatile by-products, possibly dominated by In-containing species. Previous studies have reported that the InP etch rate increases at elevated substrate temperatures [39, 40], indicating the enhanced volatility of In-containing etch by-products at higher temperatures. Notably, the rate increase observed at 80 °C occurs at a lower temperature than the 120 °C reported in our previous study, without bias voltage [16], suggesting that ion bombardment supplies additional energy that reduces the thermal activation required for higher etch rates. The IGZO film cation composition was analyzed by XPS after the qALE process at different temperatures, as shown in figure 5(b). The Ga fraction remained stable from 20 °C to 60 °C,

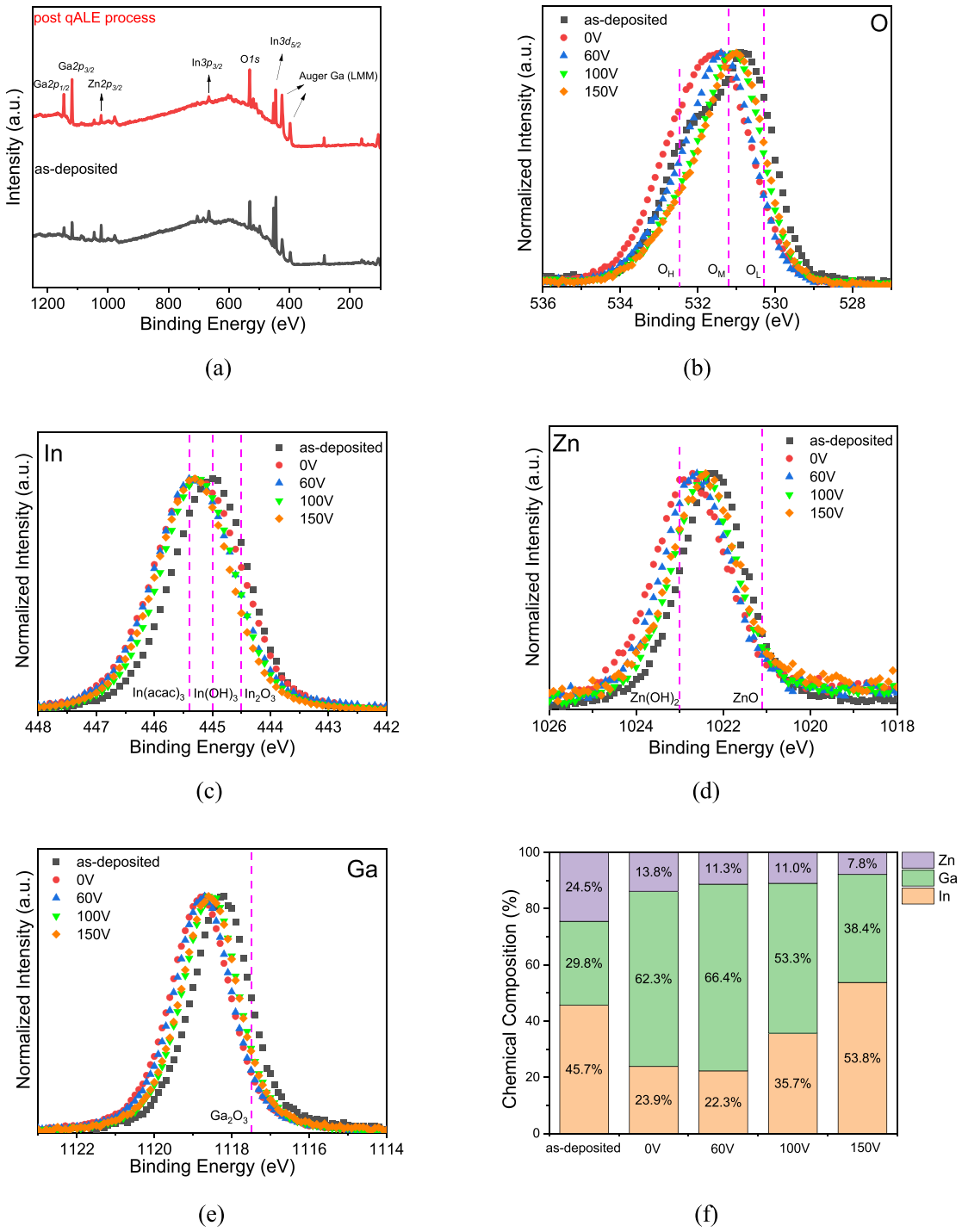

Figure 4. (a) XPS spectra of IGZO thin films before and after the quasi-ALE process, with the continuous O_2 plasma step fixed at a 60 V bias voltage. XPS spectra of (b) O 1s, (c) In 3d, (d) Zn 2p, and (e) Ga 2p at different bias voltages in the continuous O_2 plasma step. (f) IGZO cation composition before and after quasi-ALE processes at varying O_2 plasma bias voltages. The CH_4 plasma step was fixed at 30 s, the O_2 plasma step at 150 s, and the surface temperature at 140 °C in (a)–(f). The quasi-ALE process was repeated up to 20 cycles.

then increased slightly from 64.1% to 66.2% at 80 °C before stabilizing again up to 140 °C. The In fraction was stable from 20 °C to 60 °C, decreased from 24.2% to 22.7% at 80 °C, and then remained constant thereafter. The Zn fraction showed negligible change over the entire temperature range. The cation composition variations observed at 80 °C align with the etch rate increase at the same temperature and suggest an enhanced In etch rate at higher surface temperature, likely due to a stronger chemical etching contribution to In removal, which is consistent with our previous observations in figure 4(f).

Pulsed O_2 plasmas were applied during the desorption step to define a process window for the qALE process. The total, physical, and chemical cyclic etch rates were determined for different CH_4 plasma

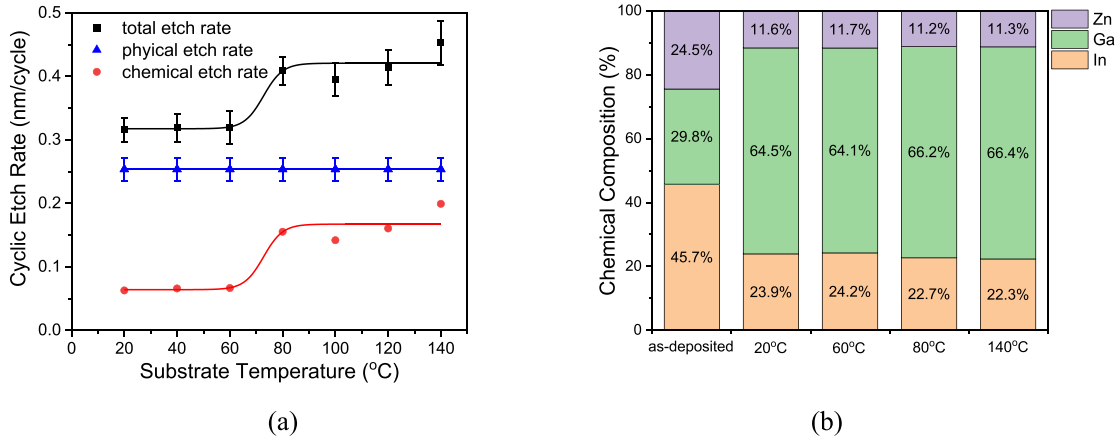

Figure 5. (a) IGZO cyclic etch rates (total, physical, and chemical) as a function of surface temperature, with the CH_4 plasma step fixed at 30 s and the continuous O_2 plasma step fixed at 150 s and a 60 V bias voltage. (b) IGZO cation composition before and after quasi-ALE processes at varying surface temperatures.

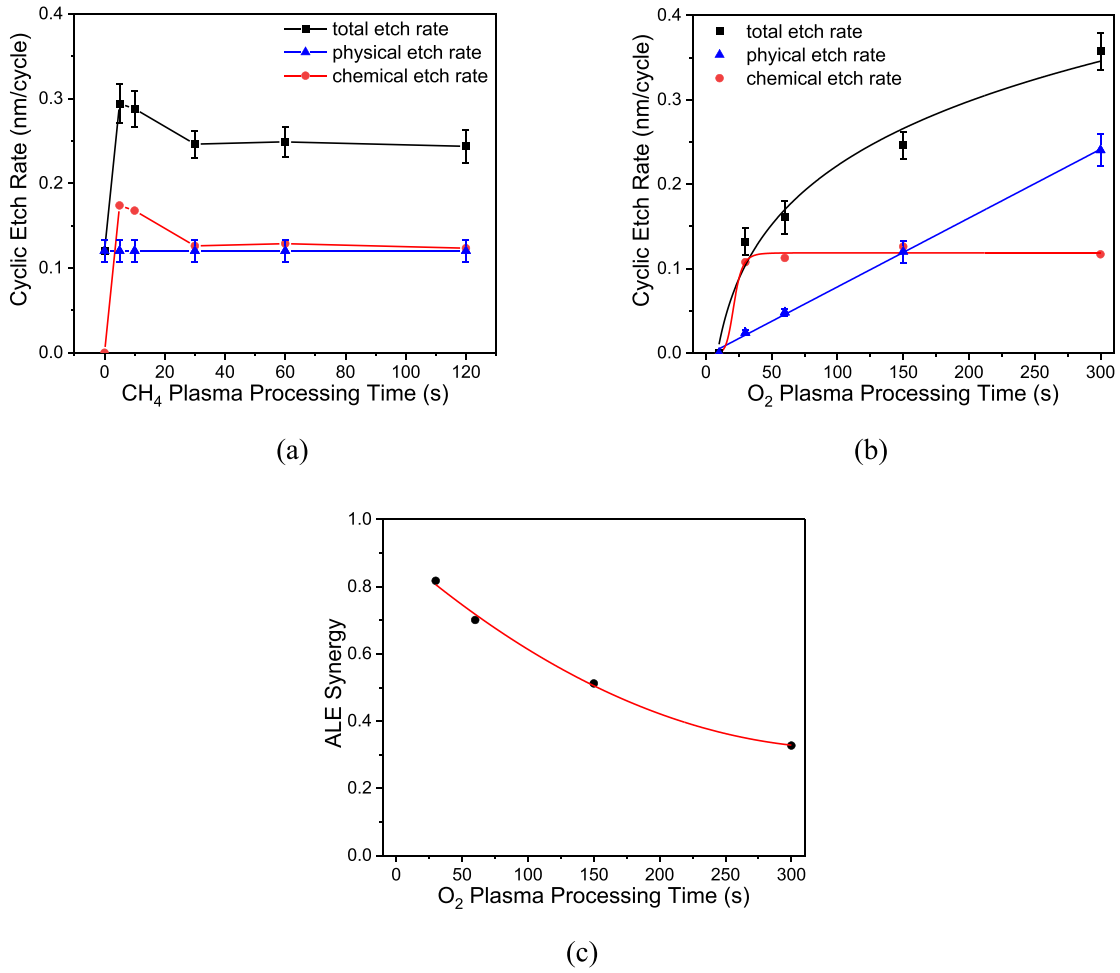

Figure 6. (a) IGZO cyclic etch rates (total, physical, and chemical) as a function of CH_4 plasma processing time, with the pulsed biased O_2 plasma step fixed at 60 V bias voltage, 45% duty cycle, and 150 s processing time. (b) IGZO cyclic etch rates (total, physical, and chemical) as a function of pulsed O_2 plasma processing time at 60 V bias voltage and 45% duty cycle, with the CH_4 plasma step fixed at 30 s. (c) ALE synergy as a function of pulsed biased O_2 plasma processing time. The surface temperature was maintained at 140 °C in (a)–(c).

times in the adsorption step and O_2 plasma times in the desorption step, as shown in figures 6(a) and 6(b). In figure 6(a), with CH_4 plasma time increasing from 5 to 120 s and a fixed 150 s pulsed O_2 plasma time with a 45% duty cycle, the total etch rate remained nearly constant at 0.25 nm/cycle. The constant etch rate is a result of the saturated thickness of the hydrocarbonated IGZO layer, which is

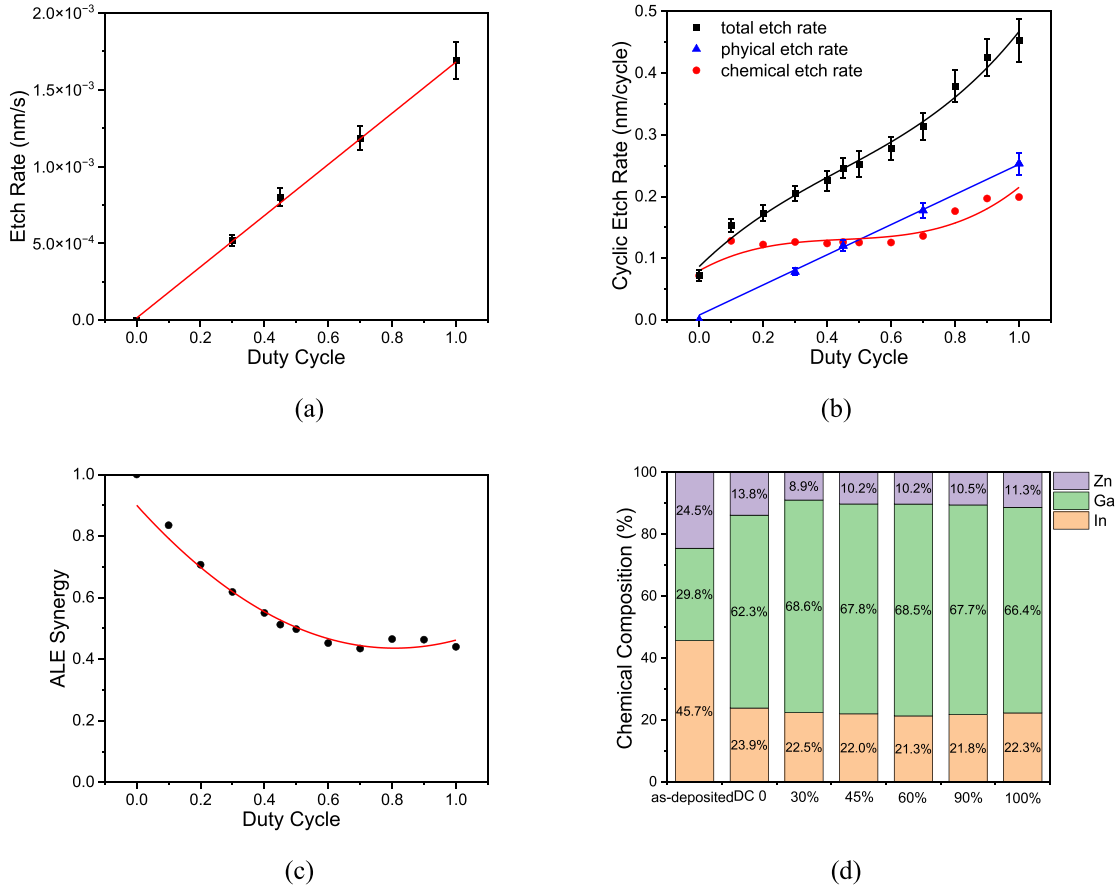

Figure 7. (a) IGZO etch rate in pulsed biased O_2 plasma at 60 V bias voltage, without the CH_4 plasma step. (b) IGZO cyclic etch rates (total, physical, and chemical) as a function of duty cycle in the pulsed biased O_2 plasma step, with the CH_4 plasma step fixed at 30 s and the O_2 plasma step fixed at 60 V bias voltage and 150 s processing time. (c) ALE synergy as a function of duty cycle in the O_2 plasma step. (d) IGZO cation composition before and after quasi-ALE processes at varying duty cycles in the O_2 plasma step. The surface temperature was maintained at 140 °C in (a)–(d).

selectively removed by O radicals during the O_2 plasma step. This value is higher than the proportionally calculated 0.20 nm/cycle from the continuous O_2 plasma etch rate (0.45 nm/cycle, figure 2(a)), due to the constant chemical etch rate within the qALE process window, discussed in the next paragraph. Slightly higher etch rates were observed at CH_4 plasma times of 5 and 10 s, similar to those under continuous O_2 plasma (figure 2(a)), which is likely due to reduced hydrocarbon deposition on the IGZO surface. The corresponding physical and chemical cyclic etch rates were 0.12 nm/cycle and 0.13 nm/cycle, respectively. The cyclic etch rate as a function of pulsed O_2 plasma time is shown in figure 6(b). As with continuous O_2 plasma, the physical cyclic etch rate increased linearly with pulsed O_2 plasma time, while the chemical cyclic etch rate rose to 0.11 nm/cycle at 30 s before saturating with further exposure. The ALE synergies under different O_2 plasma times are presented in figure 6(c). ALE synergy decreased from 0.82 at 30 s to 0.33 at 300 s, both values being higher than those observed under continuous O_2 plasma (figure 2(c)), due to the shorter plasma-on time and reduced physical sputtering in pulsed O_2 plasmas.

The dependence of IGZO cyclic etch rate, ALE synergy, and cation composition on the duty cycle of pulsed biased O_2 plasmas (desorption step) was investigated, as shown in figure 7. The IGZO etch rate increased linearly with the duty cycle of pulsed 60 V O_2 plasma without CH_4 plasma pretreatment (figure 7(a)), and correspondingly, the physical cyclic etch rate in the qALE process also scaled linearly with duty cycle (figure 7(b)). The chemical cyclic etch rate increased from 0.07 nm/cycle at 0% duty cycle to 0.13 nm/cycle at 10%, remained constant from 10%–70%, and further increased to 0.20 nm/cycle at 100%. The qALE chemical etch process window was defined between 10% and 70% duty cycle, likely corresponding to the complete removal of the saturated hydrocarbonated IGZO layer under moderate ion bombardment. The ALE synergy decreased from 1.0 at 0% duty cycle to 0.45 at 60% and remained nearly constant up to 100% (figure 7(c)). The IGZO cation composition as a function of pulsed O_2 plasma duty cycle is shown in figure 7(d). The Ga fraction increased from 62.3% at 0% duty cycle to 68.6% at 30% before stabilizing up to 100%. The Zn fraction decreased from 13.8%

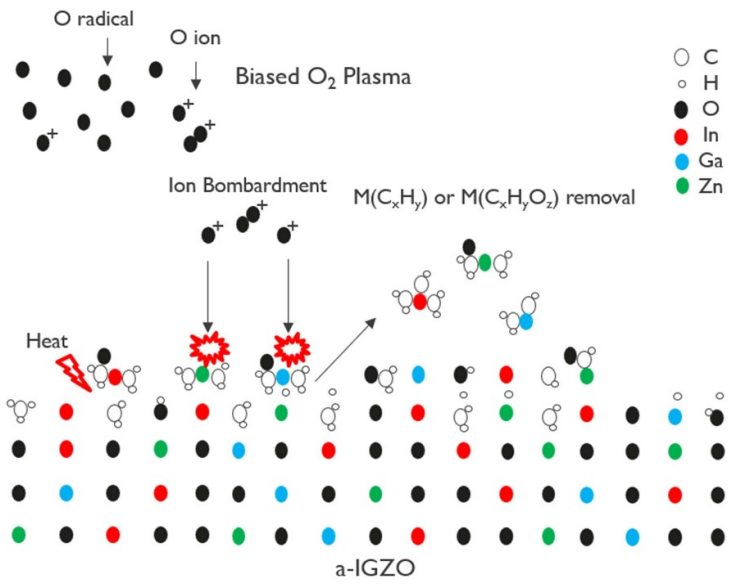

Figure 8. A simplified schematic of the IGZO qALE process in the biased O_2 plasma step.

at 0% duty cycle to 8.9% at 30% and then remained constant, while the In fraction showed negligible change across the full range.

The potential IGZO etch mechanism underlying this qALE process is proposed based on the preceding analyses. During the unbiased CH_4 plasma step, a hydrocarbon layer is deposited on the IGZO surface, while hydrocarbon and hydrogen radicals penetrate into the IGZO film. Oxygen atoms in the IGZO matrix with low bond energies can be removed in the form of H_2O and CO, creating oxygen vacancies that promote the incorporation of hydrocarbons into the IGZO matrix. The thickness of this hydrocarbonated IGZO layer increases with CH_4 plasma processing time and eventually saturates [16], leading to the self-limiting behavior of the chemical etch component in this qALE process. Subsequently, during the biased O_2 plasma step, O radicals remove excess hydrocarbons and facilitate the formation of etch by-products such as $M(C_xH_yO_z)$ (where M represents In, Ga, or Zn) or $M(C_xH_y)$ [16], as illustrated in a simplified schematic in figure 8. These etch by-products are desorbed from the surface through energy supplied by ion bombardment and substrate heating. The formation and desorption of Ga- and Zn-containing etch by-products are enhanced by increased ion bombardment, whereas In-containing etch by-products are more readily formed and desorbed at elevated substrate temperatures. Once the hydrocarbonated IGZO layer is completely removed, continued exposure to O_2 plasma can etch the underlying pristine IGZO layer via the physical component of this qALE process if the ion bombardment is not sufficiently moderated.

The etch profiles of the top gate trench in IGZO-based devices were examined by TEM after processing with the qALE technique, as shown in figure 9. After 15 cycles of this anisotropic qALE process, the 4 nm In_2O_3 layer and part of the 7 nm IGZO layer were etched. The etch profile obtained under a qALE process with low ALE synergy (figure 9(a)) exhibited substantial sidewall residues, a sloped etch front and noticeable rounding at the top of the patterned structure, attributed to strong physical sputtering under low-synergy conditions. The etch by-products produced by physical sputtering are non-volatile and redeposit on the sidewalls. These residues hinder further etching, resulting in a sloped etch front. Moreover, a process with a strong physical etch component typically shows low etch selectivity, which can cause SiO_2 etch and lead to the rounded top of the patterned structure. To improve the etch profile, a high synergy qALE process was applied. With a dominant chemical etch component and volatile etch by-products, the high synergy process produces clean sidewalls, a straight etch front, and minimal top rounding, as shown in figure 9(b). Furthermore, the IGZO channel thickness can be precisely controlled by adjusting the number of qALE cycles, meeting the critical requirement for accurate channel thickness tuning in scaled device fabrication and thereby ensuring consistent and reliable electrical performance of IGZO-based devices.

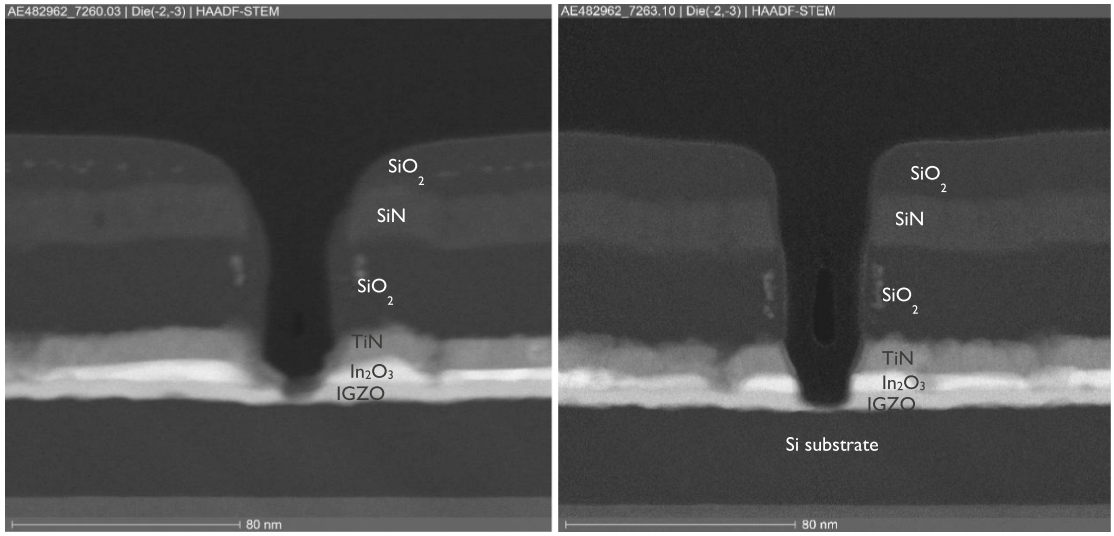

(a) (b)

Figure 9. Cross-sectional TEM images of the gate trench in the IGZO channel device using quasi-ALE processes with (a) a low ALE synergy and (b) a high ALE synergy. The 4 nm In_2O_3 layer and part of the 7 nm IGZO layer were etched using the anisotropic quasi-ALE process.

4. Conclusion

In this study, an anisotropic qALE process for IGZO removal was developed, combining alternating unbiased CH_4 plasma adsorption and biased (continuous or pulsed) O_2 plasma desorption steps. The total cyclic etch rate was analyzed in terms of its physical and chemical components. The physical component increased linearly with O_2 plasma processing time, bias voltage, and pulse duty cycle, while the chemical component was observed to be self-limiting as the CH_4 and O_2 plasma processing times increased. The chemical cyclic etch rate increased from 0.07 nm/cycle at 0% duty cycle in pulsed biased O_2 plasma to 0.13 nm/cycle at 10%, remained constant from 10% to 70%, and further increased to 0.20 nm/cycle at 100%, defining a qALE process window between 10% and 70% duty cycle at a 60 V bias voltage. ALE synergy decreased with increasing O_2 plasma time, higher bias voltage, and higher duty cycle, due to the enhanced physical etching. XPS analysis of the IGZO film surface revealed that the Ga fraction increased following the qALE process, whereas at higher O_2 plasma bias voltages, the Ga enrichment was less pronounced, indicating the formation and desorption of Ga-containing etch by-products under stronger ion bombardment. This anisotropic qALE process was successfully applied to top-gate trench patterning for IGZO channel transistor fabrication, enabling precise control of the channel thickness and achieving excellent etch profiles with high ALE synergy.

Acknowledgment

We acknowledge the support of IMEC's pilot line and MCA team for their contributions to the deposition and characterization processes. This work has been enabled in part by the NanoIC pilot line. The acquisition and operation are jointly funded by the Chips Joint Undertaking, through the European Union's Digital Europe (101183266) and Horizon Europe programs (101183277), as well as by the participating states Belgium (Flanders), France, Germany, Finland, Ireland and Romania.

Data availability statement

All data that support the findings of this study are included within the article (and any supplementary files).

Author contribution

Jie Li 0009-0005-0093-537X
Conceptualization (lead), Data curation (lead), Formal analysis (lead), Investigation (lead), Methodology (lead), Validation (lead), Writing – original draft (lead), Writing – review & editing (lead)

References

[1] Belmonte A *et al* 2020 Capacitor-less, long-retention (>400s) DRAM cell paving the way towards low-power and high-density monolithic 3D DRAM *2020 IEEE Int. Electron Devices Meeting (IEDM)* 28.2.1–28.2.4

[2] Lu W *et al* 2022 First demonstration of dual-gate IGZO 2T0C DRAM with novel read operation, one bit line in single cell, I_{ON}=1500 μA/μm@V_{DS}=1 V and retention time>300s *IEEE Int. Electron Devices Meeting (IEDM)* vol 2022 pp 26.4.1–26.4.4

[3] Belmonte A *et al* 2021 Tailoring IGZO-TFT architecture for capacitorless DRAM, demonstrating $>10^3$s retention, $>10^{11}$ cycles endurance and L_g scalability down to 14 nm *2021 IEEE Int. Electron Devices Meeting (IEDM)* pp 10.6.1–10.6.4

[4] Tang H, Dekkers H, Rassoul N, Sutar S, Subhechha S, Afanas'ev V, Houdt J V, Delhougne R, Kar G S and Belmonte A 2024 Study of contact resistance components in short-channel indium-gallium-zinc-oxide transistor *IEEE Trans. Electron Devices* **71** 567–73

[5] Liu J *et al* 2021 Low-power and scalable retention-enhanced IGZO TFT eDRAM-based charge-domain computing *2021 IEEE Int. Electron Devices Meeting (IEDM)* pp 21.1.1–21.1.4

[6] Joo Y-H and Kim C 2015 High-density plasma etching characteristics of indium–gallium–zinc oxide thin films in CF_4/Ar plasma *Thin Solid Films* **583** 40–45

[7] Lee C-Y 2021 Etching characteristics and changes in surface properties of IGZO thin films by O_2 addition in CF_4/Ar plasma *Coatings* **11** 906

[8] Park J C, Jeong O G, Kim J K, Yun Y-H, Pearton S J and Cho H 2013 Comparison of chlorine- and fluorine-based inductively coupled plasmas for dry etching of $InGaZnO_4$ films *Thin Solid Films* **546** 136–40

[9] Kim K, Efremov A, Lee J, Kwon K-H and Yeom G Y 2015 Etching mechanisms of (In, Ga, Zn)O thin films in CF_4/Ar/O_2 inductively coupled plasma *J. Vac. Sci. Technol. A* **33** 031601

[10] Joo Y-H, Woo J-C and Kim C-I 2012 A study of the surface chemical reactions on IGZO thin film in BCl_3/Ar inductively coupled plasma *J. Electrochem. Soc.* **159** D190–5

[11] Kwon K-H, Efremov A, Kang S, Jang H, Yang H and Kim K 2012 Etching behavior and mechanism of In- and Ga-doped ZnO thin films in inductively coupled BCl_3/Cl_2/Ar plasmas *Jpn. J. Appl. Phys.* **51** 076201

[12] Shin D-C, Park K-S, Park B-R, Choe H, Jeon J-H, Lee K-W and Seo J H 2011 A study on the dry etching characteristics of indium gallium zinc oxide and molybdenum by the CCP-RIE system for the 4 mask process *Curr. Appl. Phys.* **11** S45–S48

[13] Kundu S, Decoster S, Bezard P, Nalin Mehta A, Dekkers H and Lazzarino F 2022 High-density patterning of InGaZnO by CH_4: a comparative study of RIE and pulsed plasma ALE *ACS Appl. Mater. Interfaces* **14** 34029–39

[14] Hong J W *et al* 2024 Reactive ion etching of indium gallium zinc oxide (IGZO) and chamber cleaning using low global warming potential gas *Appl. Surf. Sci.* **671** 160692

[15] Li J, Kundu S, Souriau L, Bezard P, Izmailov R and Lazzarino F 2025 Plasma etch of IGZO thin film and IGZO/SiO_2 interface diffusion in inductively coupled CH_4/Ar plasmas *Plasma Process. Polym.* **22** 2400186

[16] Li J, Kundu S, Souriau L, Belmonte A and Devriendt K 2025 Atomic layer etching of InGaZnO thin films via plasma hydrocarbonation and oxygen radical reaction *Plasma Sources Sci. Technol.* **34** 085001

[17] Kanarik K J *et al* 2017 Predicting synergy in atomic layer etching *J. Vac. Sci. Technol. A* **35** 05C302

[18] Lopaev D V, Rakhimova T V, Rakhimov A T, Zotovich A I, Zyryanov S M and Baklanov M R 2018 Silicon dioxide and low-k material sputtering in dual frequency inductive discharge by argon ions with energies from 16 to 200 eV *J. Phys. D: Appl. Phys.* **51** 02LT02

[19] Ozer C, Ebeoglugil M F, Yildirim S and Nil M 2022 High-performance a-IGZO-based flexible TTFT with stacked dielectric layers via ultrathin high-k $SrTiO_3$ buffer layer grown on HfO_2 *Mater. Sci., Mater. Electron.* **33** 1511–28

[20] Cho D-Y, Song J, Shin Y C, Hwang C S, Choi W S and Jeong J K 2009 Influence of high temperature postdeposition annealing on the atomic configuration in amorphous In-Ga-Zn-O films *Electrochem. Solid State Lett.* **12** H208–10

[21] Jeong H, Lee B, Lee Y, Lee J, Yang M, Kang I, Mativenga M and Jang J 2014 Coplanar amorphous-indium-gallium-zinc-oxide thin film transistor with He plasma treated heavily doped layer *Appl. Phys. Lett.* **104** 022115

[22] Wang Y, Zhou Y, Xia Z, Zhou W, Zhang M, Yeung F S Y, Wong M, Kwok H S, Zhang S and Lu L 2022 Compact integration of hydrogen-resistant a-InGaZnO and poly-Si thin-film transistors *Micromachines* **13** 839

[23] Kim H J, Tak Y J, Park S P, Na J W, Kim Y, Hong S, Kim P H, Kim G T, Kim B K and Kim H J 2017 The self-activated radical doping effects on the catalyzed surface of amorphous metal oxide films *Sci. Rep.* **7** 12469

[24] Mativenga M, Haque F, Billah M M and Um J G 2021 Origin of light instability in amorphous IGZO thin-film transistors and its suppression *Sci. Rep.* **11** 14618

[25] Hong S, Park S P, Kim Y, Kang B H, Na J W and Kim H J 2017 Low-temperature fabrication of an HfO_2 passivation layer for amorphous indium-gallium-zinc oxide thin film transistors using a solution process *Sci. Rep.* **7** 16265

[26] Huang X, Wu C, Lu H, Ren F, Chen D, Liu Y, Yu G, Zhang R, Zheng Y and Wang Y 2014 Large-swing a-IGZO inverter with a depletion load induced by laser annealing *IEEE Electron Device Lett.* **35** 1034–6

[27] Chen M, Pei Z L, Sun C, Wen L S and Wang X 2000 Surface characterization of transparent conductive oxide Al-doped ZnO films *J. Cryst. Growth* **220** 254–62

[28] Fan J C C and Goodenough J B 1977 x-ray photoemission spectroscopy studies of Sn-doped indium-oxide films *J. Appl. Phys.* **48** 3524–31

[29] Kim M G, Kim H S, Ha Y G, He J, Kanatzidis M G, Facchetti A and Marks T J 2010 High-performance solution-processed amorphous zinc-indium-tin oxide thin-film transistors *J. Am. Chem. Soc.* **132** 10352–64

[30] Donley C, Dunphy D, Paine D, Carter C, Nebesny K, Lee P, Alloway D and Armstrong N R 2002 Characterization of indium-tin oxide interfaces using x-ray photoelectron spectroscopy and redox processes of a chemisorbed probe molecule: effect of surface pretreatment conditions *Langmuir* **18** 450–7

[31] Kim J S, Ho P K H, Thomas D S, Friend R H, Cacialli F, Bao G-W and Li S F Y 1999 x-ray photoelectron spectroscopy of surface-treated indium-tin oxide thin films *Chem. Phys. Lett.* **315** 307–12

[32] Nomura K, Kamiya T, Ohta H, Uruga T, Hirano M and Hosono H 2007 Local coordination structure and electronic structure of the large electron mobility amorphous oxide semiconductor In-Ga-Zn-O: experiment and ab initio calculations *Phys. Rev. B* **75** 035212

[33] Lee J C *et al* 2025 Identifying the chemical structure of indium-gallium-zinc oxide thin films with oxygen vacancy variation *ACS Appl. Electron. Mater.* **18** 8393–9

[34] Idriss H 2021 On the wrong assignment of the XPS O1s signal at 531–532 eV attributed to oxygen vacancies in photo- and electrocatalysts for water splitting and other materials applications *Surf. Sci.* **712** 121894

[35] Li J, Nolan M and Detavernier C 2023 A step toward correct interpretation of XPS results in metal oxides: a case study aided by first-principles method in ZnO *J. Chem. Phys.* **159** 034702
[36] Auewattanapun K, Bermundo J P S, Hanifah U, Nakajima H, Limphirat W, Techapiesancharoenkij R and Uraoka Y 2024 Spectroscopic analysis of electrical phenomena and oxygen vacancy generation for self-aligned fully solution-processed oxide thin-film transistors *ACS Appl. Mater. Interfaces* **16** 60521–9
[37] Kamiya T, Nomura K and Hosono H 2010 Subgap states, doping and defect formation energies in amorphous oxide semiconductor a-$InGaZnO_4$ studied by density functional theory *Phys. Status Solidi* **207** 1698–703
[38] Melville D L, Simmons J G and Thompson D A 1993 Identification of volatile products in low pressure hydrocarbon electron cyclotron resonance reactive ion etching of InP and GaAs *J. Vac. Sci. Technol. B* **11** 2038–45
[39] Youtsey C, Grundbacher R, Panepucci R, Adesida I and Caneau C 1994 Characterization of chemically assisted ion beam etching of InP *J. Vac. Sci. Technol. B* **12** 3317–21
[40] Dultsev F N and Kesler V G 2009 Etching and oxidation of InAs in planar inductively coupled plasma *Appl. Surf. Sci.* **256** 246–50